Universität Potsdam
Institut für Physik und Astronomie

Bachelor thesis

X-raying winds of blue supergiant stars with the XMM-Newton Space Telescope

by Lea Faber
matricle number: 790519

July 7, 2021

first exmaniner: Prof. Dr. Lidia Oskinova
second examiner: PD Dr. Axel Schwope

Contents

1 Introduction

Blue supergiant stars (BSGs) are massive, hot and luminous stars, which are in an advanced state in their evolution. They start their lives with masses $M_{\text{initial}} \geq 10 M_{\odot}$ and have the luminosity class I, which has the subcategories a and b. The stars considered in this work have an effective temperature range of $18000K$ to $30000K$, masses above $20 M_{\odot}$ and corresponding spectral types B0 to B2.

Some of the brightest stars of our night sky that can be seen by the naked eye are BSGs, like ϵ Ori or γ Ara, which are both included in this thesis. BSGs have already evolved off the main sequence, where they started as O or early-B type dwarf stars. In comparison to stars with lower masses, their lives are relatively short. They are among the progenitors of supernovae (SN) and might collapse into neutron stars (NSs) or black holes (BHs) at the end of their evolution. The need to understand BSGs increased due to the recent detection of gravitational waves from coalescing BHs and NSs. Also the supernova SN 1987A, which progenitor star was a BSG, gave reasons for further studies. The explosion of the star wasn't predicted by any theory and even though it is a core-collapse supernova a neutron star couldn't be detected in the supernova remnant yet. It is clear that there are many questions about BSGs remain unanswered. They might be just a small group of stars, but they are influential and many physical processes in them are not understood.

One of the most important processes in the evolution of BSGs are their stellar winds, which are transferring matter, energy and momentum into the interstellar medium (ISM). The removal of mass by stellar wind can determine if the star will become a black hole or a neutron star at the end of its live. Searle et al. (2008), for example, has fitted H_{α}-lines in spectra of 20 BSGs and on this basis derived mass loss rates in orders between 10^{-8} and $10^{-6} M_{\odot}\,\mathrm{yr}^{-1}$. However there are still huge differences between empirically derived and theoretical predicted mass loss rates.

Stellar wind theory predicts a dependency of wind strength on stellar effective temperature and consequently on spectral subtype. Between early and later subtypes of BSGs is a huge drop in the wind strength, which is called the bi-stability jump, which was first described by Lamers et al. (1995). This jump is so interesting, because it changes the character of the wind itself. While on the hot side of the jump the winds are driven by Fe III ionisation, the temperature on the cooler side is not high enough for ionisation of Fe III any more. Studying the winds of stars with temperatures on both sides of the bi-stability jump could help to clear the processes driving the stellar winds.

Nearly all massive stars emit x-rays, including BSGs. Since OB stars were first observed by the Einstein observatory (Seward et al., 1979; Harnden et al., 1979) as x-ray sources x-ray telescopes open a high-energy window for stellar wind studies, because the source of the x-ray emission from massive stars seems to be their stellar winds. For the first time we now can look into this with the biggest x-ray telescopes, like the XMM-Newton space

telescope of the European Space Agency (ESA) [1] or the Chandra x-ray observatory of the National Aeronautics and Space Administration (NASA) [2]. In this thesis the BSGs on both sides of the bi-stability jump are addressed using x-ray spectroscopy. The goal is to determine how x-ray properties depend on spectral type and by establishing that, to confront stellar wind theory and the models of x-ray production in stellar winds.

[1] https://www.cosmos.esa.int/web/xmm-newton
[2] https://chandra.harvard.edu

2 Blue supergiants stars and their stellar winds

Figure 1 shows the upper Herzsprung-Russel-diagram (HRD) where the massive stars are located. Unlike stars with lower masses, which cross the HRD just one time before exploding, massive stars along in the green line or above in figure 1 can cross the HRD two times. It is still not known if a BSG is evolving toward higher or lower temperatures when it is placed on the HRD.

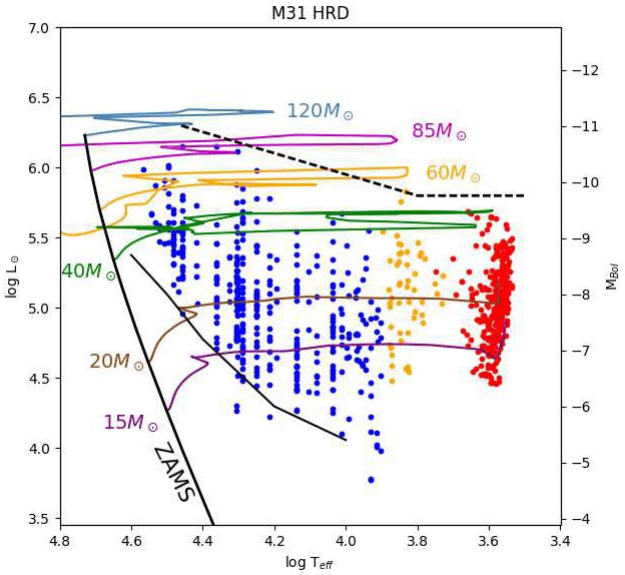

Figure 1: The Hertzsprung-Russel diagram for massive stars in galaxy M31 with evolutionary tracks, displayed as coloured lines with the initial masses of the stars shown next to them and the zero-age-main-sequence (ZAMS) from Ekström et al. (2012). Taken into account in the evolutionary tracks are the mass loss of the stars, a Milky Way metalicity and no rotation. The dashed line shows the Humphreys–Davidson (H–D) limit. OBA supergiants are displayed in blue, yellow supergiants (YSGs) are yellow and red supergiants (RSGs) are red. The figure is adapted from Humphreys et al. (2017).

To expand our knowledge of stellar evolution it is necessary to understand stellar winds, whose resulting mass loss rates $\dot{M}$ $[M_\odot\,\mathrm{yr}^{-1}]$ are among the key factors governing massive star evolution. Stellar winds also impact the evolution of the ISM. The winds of early B-type supergiants are also interesting because of the possibility to use them for measuring extra-galactic distances using the Wind-Momentum-Luminosity-Relation (WLR) (Kudritzki, 1999).

Stellar winds are streams of matter that are moving away from a star. In BSGs it consists mostly of hydrogen (H) and helium (He) as well as trace metals. While in solar type

stars the stellar winds are not really strong with mass loss rates of $\dot{M}_{\rm sun} \sim 10^{-12} M_{\odot} {\rm yr}^{-1}$, the mass loss rates of BSGs are 4 to 6 orders of magnitude higher. In contrast to our sun they are driven by the radiative pressure. That means, the photons emitted by the star transfer impulse to ions, which results in a radiative pressure, that in netto is directed radially outwards. If the velocity of these particles is high enough they can escape the gravitational hold of the star. Therefore this velocity is called escape velocity $v_{\rm esc}$. The wind has a subsonic part, which is close to the photosphere. After the sonic point the velocity becomes supersonic and is often described by the β-velocity law, which means that it increases with distance r until it reaches the terminal velocity v_{∞}.

$$v(r) = v_{\infty} \left(1 - \frac{R_*}{r}\right)^{\beta} \tag{1}$$

Most of the times it is assumed that β is between 0.5 and 1.5 (e.g. Vink et al., 1999).

The velocity of the stellar winds is closely linked to the density. The connection between these quantities lies in the continuity equation $v\rho = \text{const.} \equiv 4\pi\dot{\rm M}$, so if the density of the wind decreases, the velocity increases or vice versa.

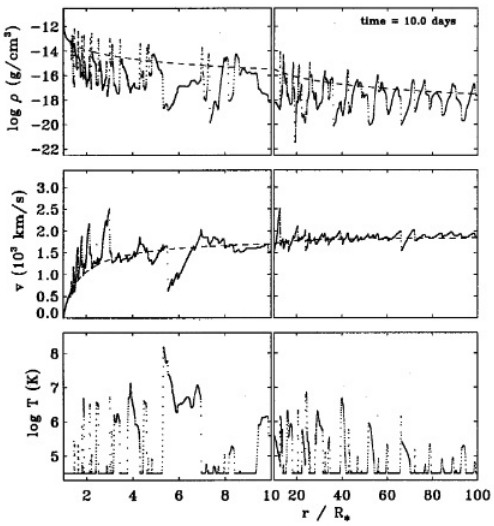

Fig. 6. Snapshot out to 100 stellar radii of the wind perturbed by a tunable photospheric sound wave. The density, velocity, and temperature are marked at each numerical grid point. The dashed line corresponds to a stationary wind with $\beta = 0.8$ velocity law.

Figure 2: The figure and the caption are adapted from Feldmeier et al. (1997).

The theory predicts that the radiatively driven stellar winds are unstable. The models from Feldmeier et al. (1995) show that the instability of line driven winds results in shock waves. Those heat the shocked part of the stellar wind up to millions degrees. However the models predicting the shockwaves are just one dimensional. Until today these are the most complete models, because transferring them to three dimensions is still too complex. Figure 2 illustrates the shockwaves and the corresponding heating of the plasma. Verifying the accuracy of this model for the stellar wind of an actual star, whose wind in reality is three dimensional, can just be done empirically at the moment.

2.1 Decline in the velocity of stellar winds in BSGs: Bi-Stability jump

The velocity of BSG stellar winds are empirically derived from the analysis of stellar UV spectra. It was noticed that a huge drop in velocity occurs near the spectral type B1. Lamers et al. (1995) had found that the velocities drop from $\frac{v_\infty}{v_{\rm esc}} = 2.6$ at the hot side to $\frac{v_\infty}{v_{\rm esc}} = 1.3$ on the cold side of bi-stability jump.

The dependence of v_∞ to spectral subtype is shown in figure 3. The drop in velocity around spectral type B1 can clearly be seen. The mean terminal velocities v_∞ for my sample of stars are displayed in table 3.

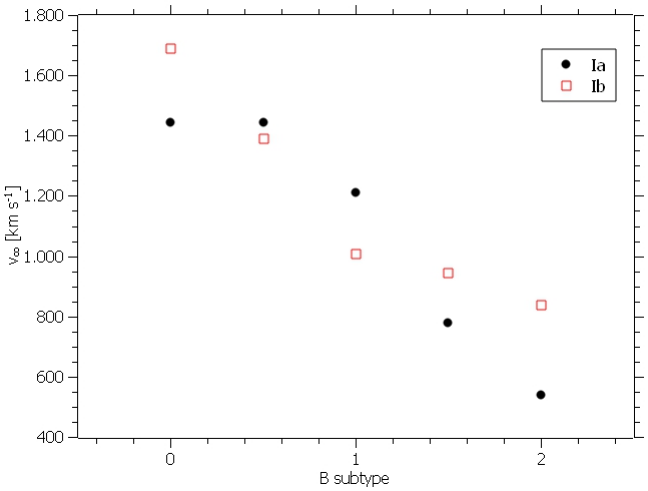

Figure 3: Dependence of the terminal velocity on spectral type with values from Prinja and Massa (1998).

Models from Pauldrach and Puls (1990) for the star P Cygni suggested that $\dot{M}v_\infty$ is constant over the jump. That would mean that $\dot{M}$ increases when v_∞ decreases. This suggestion was tested in models in Vink et al. (1999) and indeed they could find an accompanying jump in mass loss rate $\dot{M}$. These models determine an increase of circa factor 5 between $T_{\rm eff} = 27500$ K and $T_{\rm eff} = 20000$ K in $\dot{M}$. Below and above this range $\dot{M}$ decreases with $T_{\rm eff}$.

The mass loss rate is driven by spectral lines, therefore an increase in line force is needed for an accompanying increase in $\dot{M}$. With that Vink et al. (1999) explains the origin of the bi-stability jump in $\dot{M}$ with a change of the ionization balance of Fe III in hot star winds. The Vink et al. (1999) models need to be verified empirically. However, it is notoriously difficult to measure mass loss rates in BSGs. The term "bi-stability" connects the behaviour of v_∞ and $\dot{M}$ by reflecting the fact that two stable solutions are possible for the stellar wind dynamics: fast and thin winds or slow and thick winds.

Still one of the problems in calculating mass loss rates are the differences in values for models like Vink et al. (1999) and calculations from fitting H_α-lines in observed data. In general it seems that $\dot{M}_{\mathrm{vink}} > \dot{M}_{H_\alpha}$ for spectral types B1 and later subtypes, while for O-type star it's the other way around. Petrov et al. (2014) modelled the H_α-line for stars with different T_{eff} and found a maximum in equivalent width (EW) in the region of the bi-stability jump and a possible change in character of the H_α-line over the jump, which could explain the differences between the empirically derived and theoretical predicted mass loss rates. There are also current models suggesting that the increase in $\dot{M}$ over the jump results in a slower rotation of the star. This is called bi-stability braking (BSB) (Vink et al., 2010).

Lamers et al. (1995), also mentioned the possibility of a second jump near $T_{\mathrm{eff}} \sim 10000$K, but this hasn't been confirmed yet. There are also observations, which lead to speculations, that B giants also go through a bi-stability jump even though their mass loss rates $\dot{M}$ are predicted to be at least ten times smaller than in BSGs.

2.2 X-ray emission

From most massive stars, we can detect x-ray emission. The effective temperature of the star itself is not sufficient to explain the observed x-ray luminosities. Now it is assumed, that the x-rays result from highly heated plasma parts in their stellar wind, which are due to shockwaves. Lucy and White (1980) first suggested that x-rays from massive stars are due to dynamic processes in their stellar winds and later on Feldmeier et al. (1997) with their one dimensional radiative hydrodynamic models demonstrated that stellar wind shocks could be the source of x-ray emission in O stars.

The part of stellar winds heated by shocks can be described as collisional, optically-thin, hot plasma. In those plasmas x-ray emission occur due to recombination and Bremsstrahlung.

The atoms collide and get ionized or excited. When the electron recombines or falls back to a lower energy level in the atom, a photon gets emitted. It applies here that the electron temperature is proportional to the ionization energy of the photons $kT_{\mathrm{e}} \propto I_{\mathrm{p}}$. Emission due to recombination can occur in two ways, radiative and dielectronic recombination. Is the ionized atom with which the electron recombines in an excited state, emission can occur as dielectronic recombination, when the recombining electron excites another electron. Satellite lines occur when the excited electron changes to a lower energy level and because of the excited recombined electron the wavelength of the emitted photon is a bit longer than the normal line emission. When the electron autoionizes instead, the process can be compared to scattering.

To calculate the emissivity it is important to know the ionization balance of the plasma. Emissivity of spectral lines is dependent on electron density n_{e} and temperature T of the

plasma as well as the ion densities n_{i}. Collisional ionization equilibrium (CIE) plasmas are types of plasma typically found in stellar winds and coronae. The dedicated codes, such as APEC (Smith et al., 2001) can be used for spectral analysis.

Another relevant mechanism of x-ray emission in this plasma is the Bremsstrahlung. It gets produced when a charged particle changes its velocity because it loses energy by getting deflected by another charged particle. The loss in energy is converted into the emission of a photon. Since both particles aren't bound it is often referred to as free-free radiation. The wavelength of the photon depends on the energy loss. Therefore it is a continuum radiation. This is mostly important in optically thin plasma and therefore relevant in stellar winds.

The resulting spectrum is a combination of the recombination and de-excitation and the emission due to Bremsstrahlung. Black body emission isn't relevant in optically-thin plasmas because it only occurs when the photons get trapped inside the plasma.

2.2.1 Predicting the temperature of hot gas in stellar wind from basic considerations

A shock wave or contraction wave in a one dimensional flow in a fluid can be divided in two regions, before and after the shock. The connection between these two regions is described by the Rankine-Hugoniot condition. It expresses the conversation of mass, momentum and energy. In theory the plasma temperatures due to the shock waves is proportional to the amplitude of the velocity jump. Equation 3 shows the connection between those two variables with help of the Rankine-Hugoniot condition

$$kT_{\mathrm{X}} = \frac{3}{16} m_{\mathrm{H}} \mu v^2 \tag{2}$$

with $m_{\mathrm{H}} = 1 \cdot 10^{-24}$g and in the case of hydrogen plasma μ=0.5. For the stellar winds of BSGs this value is adopted (in equation 3) because in the winds the main source of electrons comes from ionized hydrogen. In reality μ is slightly higher than 0.5, but to estimate it correctly it would be necessary to know how strong the metals in the wind are ionized. For the stellar winds of BSGs equation 2 could be expressed as

$$T_{\mathrm{s}}\ [\mathrm{MK}] = 14 \left(\frac{\mathrm{v}_\infty\ [\mathrm{km\,s^{-1}}]}{1000} \right)^2, \tag{3}$$

where the maximum amplitude for the velocity jump is adopted.

2.2.2 Estimating the x-ray luminosity

Another important parameter in x-ray emission is the x-ray flux and the corresponding x-ray luminosity. Luminosity describes the amount of light that gets emitted from a

source in energy per second. It depends on the Emission Measure EM [cm^{-3}] and a cooling function $\Lambda(E)$ [erg cm^3 s^1].

$$L_\mathrm{X} = EM\ \Lambda(E) \tag{4}$$

$$\text{with } EM = \int_V n_e n_i \mathrm{d}V \tag{5}$$

with n_e as electron column density and n_i as ion column density. These can be expressed via density as

$$n_\mathrm{e} n_\mathrm{i} = \frac{\rho^2}{\mu_\mathrm{e} \mu_i^; m_\mathrm{H}^2} \tag{6}$$

where μ_e and μ_i are the molecular weight per electron and per ion, m_H [g] the proton mass and $\rho = \rho(r)$, which follows the continuity equation

$$\rho(r) = \frac{\dot{M}}{4\pi r^2 v(r)}, \tag{7}$$

It is commonly assumed, that the velocity $v(r)$ follows the β-velocity law, which can be seen in equation 1. However the wind consists realistically not just of hot gas. It is a time independent, homogenous mix of "cool" ($T_\mathrm{w} \sim 10^4\,\mathrm{K}$) and "hot" ($T_\mathrm{X} \sim 10^7\,\mathrm{K}$) gas. It is spherically symmetrical and in a dynamical equilibrium. Therefore there is a filling factor which adds the ratio of cool and hot wind emission $f_\mathrm{X} = \frac{EM_\mathrm{X}}{EM_\mathrm{w}}$ where realistically $f_\mathrm{X} \ll 1$. Would all wind consist of hot gas only $f_\mathrm{X} = 1$. With equation 4, 5 and the filling factor f_X the x-ray luminosity is

$$L_\mathrm{X} = f_\mathrm{X} \Lambda_\nu(T_\mathrm{X}) \int_V n_\mathrm{e} n_\mathrm{i} e^{-\tau_\mathrm{w}} \mathrm{d}V \tag{8}$$

where τ_w is the optical depth within the stellar wind.

$$\tau_\mathrm{w} = \int_z^\infty \rho \kappa_\mathrm{w} dz, \tag{9}$$

where κ_w [$\mathrm{cm}^2\,\mathrm{g}^{-1}$] is the mass absorption coefficient and depends on the ionisation structure and chemical composition of the wind. If the optical depth would be set $\tau_\mathrm{w} = 0$, it would mean that the stellar wind doesn't absorb any x-rays. This case would lead to the maximal x-ray luminosity that could be expected. However in reality $\tau_\mathrm{w} = 0$ is not likely. Like shown later in section 6.2, it can be assumed, that the stellar wind absorbs part of the emitted x-rays again. For $\tau_\mathrm{w} \neq 0$ it is possible to do a spherical separation and divide the stellar wind in two parts, where zone 1 is $\tau_\mathrm{w} > 1$ and describes the part of the wind, that is optically too thick to contribute to the x-ray luminosity and zone 2 with $\tau_\mathrm{w} = 0$, which is optically thin. For Wolf-Rayet stars Ignace and Oskinova (1999) have already done that. In the case of spherical separation, it is possible to ignore the area near the star, where the wind is optically too thick for x-ray emission. Therefore the x-ray luminosity for the observable wind would be

$$L_\mathrm{X} \approx \frac{1}{2} 2\pi f_\mathrm{X} \Lambda_\nu(T_\mathrm{X}, E) \int_{r_1}^\infty \left(1 + \sqrt{1 - \frac{r_1^2}{r^2}}\right) n_\mathrm{e} n_\mathrm{i} r^2 \mathrm{d}r \tag{10}$$

This is called exospheric approximation and it overestimates the x-ray luminosity. Hereby the factor $1+\sqrt{1-\frac{r_1^2}{r^2}}$ is the part of the wind, that can't be seen from the line of sight of the viewer and therefore the x-rays will not be detected by a telescope. It is an occultation from the optically thick surface. Furthermore the x-ray luminosity is corrected by the prefactor $\frac{1}{2}$ to roughly account for the approximation. The radius r_1 is calculated trough K-shell photoelectronic absorption in the "cool" part of the wind, with equation 11

$$r_1 = \frac{\dot{M}}{4\pi v_\infty}\kappa(E), \tag{11}$$

where $\kappa(E)$ is the mass-absorption coefficient for the cool parts of the winds in units of [cm^2/g]. It is dependent on the energy of the photons. Now the equation 6 and 7 can be used.

$$L_\mathrm{X} \approx f_\mathrm{X}\Lambda_\nu(T_\mathrm{X},E)\frac{\pi}{\mu_\mathrm{e}\mu_i^\circ m_\mathrm{H}^2}\int_{r_1}^{\infty}\left(1+\sqrt{1-\frac{r_1^2}{r^2}}\right)\left(\frac{\dot{M}}{4\pi r^2 v(r)}\right)^2 r^2\mathrm{d}r \tag{12}$$

$$= f_\mathrm{X}\Lambda_\nu(T_\mathrm{X},E)\frac{\dot{M}^2}{\mu_\mathrm{e}\mu_i^\circ m_\mathrm{H}^2 16\pi}\int_{r_1}^{\infty}\left(1+\sqrt{1-\frac{r_1^2}{r^2}}\right)\frac{1}{r^2 v(r)^2}\mathrm{d}r \tag{13}$$

To prevent division by zero for $r = r_1$ I assume $v(r) = v_\infty$ and the velocity is therefore constant. The resulting integral can be solved analytically.

$$\int_{r_1}^{\infty}\frac{\left(1+\sqrt{1-\frac{r_1^2}{r^2}}\right)}{r^2}\mathrm{d}r = \frac{\pi+4}{4r_1} \tag{14}$$

That leads with help of equation 11 to the following equation for x-ray luminosity:

$$L_\mathrm{X} \approx \Lambda_\nu(T_\mathrm{X},E)\frac{f_\mathrm{X}\frac{\dot{M}}{v_\infty}}{\mu_\mathrm{e}\mu_i^\circ m_\mathrm{H}^2\kappa(E)}\frac{1+\frac{\pi}{4}}{4}. \tag{15}$$

The x-ray luminosity is therefore dependent not only on v_∞ and T_X, but also on $\dot{M}$ and $\kappa(E)$. To be consitent from our spectral analysis (see section 6), we retrieve the energy integrated cooling funktion $\Lambda(T_\mathrm{X})$ using the x-ray analysis software xspec. The flux can be described with the help of $\Lambda(T_\mathrm{X})$ as

$$F_\mathrm{X} = \frac{L_\mathrm{X}}{4\pi d^2} = \frac{\Lambda(E)\cdot EM}{4\pi d^2} \tag{16}$$

with d as the distance to the source. In the APEC model (see more in section 6.1), which is most suited for the stellar winds of BSGs, $norm$ is defined as $norm = \frac{10^{-14}}{4\pi d^2}\,EM$. For $\Lambda(E)$ that means, $\Lambda(E) = \frac{10^{-14}F_\mathrm{X}}{norm}$. When $norm = 1$ it is possible to create a table where $\Lambda(E) = 10^{-14}F_\mathrm{X}$, where the flux can be calculated with xspec (see table 1). The resulting function $\Lambda(T_\mathrm{X})$ [10^{-23} erg cm^3 s^{-1}] is displayed in figure 4.

Table 1: Cooling function Λ determined by setting the paramter *norm* to unity in the *apec* model

kT [keV]	$F_{\rm X}$ in 0.2-10.0 keV [10^{-9} erg cm^{-2} s^{-1}] = $\Lambda(T_{\rm X})$ [10^{-23} erg cm^3 s^{-2}]
0.2	2.46
0.4	2.87
0.6	3.45
0.8	3.43
1.0	2.93
1.2	2.35
1.4	1.98
1.6	1.80
1.8	1.72

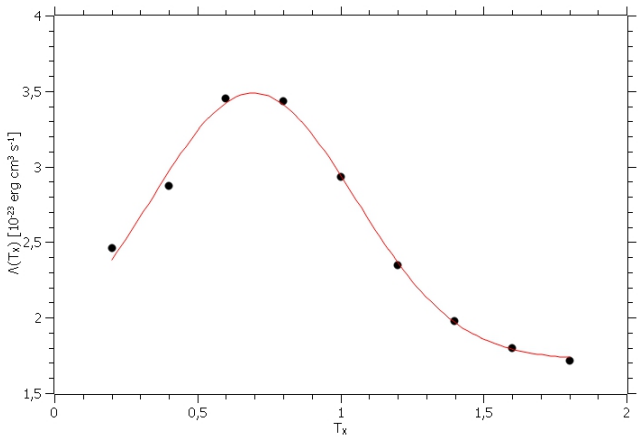

Figure 4: Cooling function $\Lambda_\nu(T_{\rm X})$ with the fit function $y_0 + A\frac{\sqrt{\frac{2}{\pi}}}{w}e^{-2\left(\frac{x-x_c}{w}\right)^2}$ and parameters A=1.6 $\pm$ 0.1; x_c = 0.70 $\pm$ 0.01; w = 0.71 $\pm$ 0.04; y_0 = 1.72 $\pm$ 0.05.

X-ray emission and their parameters like plasma temperatures and x-ray fluxes due to shockwaves in the wind are highly dependent on the wind velocity and therefore, change for stars located on both sides of the bi-stability jump. Hence, comparing the hot plasma temperatures and fluxes derived from observations with those predicted theoretically for shocks in stellar wind provides an excellent empiric test for the theory of x-ray production in winds of BSGs. With the theories on x-ray properties described in this section, one can make some predictions: velocity decreases by factor 1.7, as can be seen in the values from Prinja and Massa (1998), meaning the temperature is expected to drop by factor 3. The density is increased, which could mean that EM is higher, but the absorption is higher as well, therefore this is more difficult to predict.

3 Absorption in the interstellar medium

While photons move from emitter to observer through space it happens that some photons get absorbed due to the interstellar medium (ISM). The part of the ISM important in this work consists mostly of really cold clouds of gas and dust between stars. It contains mainly neutral hydrogen, but also other metals and molecules. To map the cold ISM it is common to use the 21cm-line emission of neutral hydrogen. The absorption in the ISM is of crucial importance to spectral analysis, because the spectrum has to be corrected accordingly. Through photoionization radiation gets absorbed, which leads to a reddening in the observed spectrum, that can be seen in the parameter $E(B-V)$.

Photoionization cross sections σ_{ISM} give the probability of photoionization, which depends on the energy of the photons and the species of the ion. To estimate the photoionization cross sections for models concerning ISM absorption it is necessary to use the sum of the cross sections of gas, grain and dust (Wilms et al., 2000). For x-ray radiation most absorption occurs in metals, because hydrogen itself has too low energy levels to absorb x-rays. Therefore the assumed metal abundances are crucial to σ_{ISM}. The observed x-ray spectrum of a source can be described as

$$I_{\mathrm{obs}}(E) = e^{-\sigma_{\mathrm{ISM}}(E) N_{\mathrm{H}}} I_{\mathrm{source}}(E) \tag{17}$$

with σ_{ISM} normalized to the total hydrogen number density N_{H} [atoms/cm^2].
In our milky way the reddening $E(B-V)$ and the extinction A_{V} are linear.

$$E(B-V) = 3.1\, A_{\mathrm{V}} \tag{18}$$

Furthermore, the observed relation between hydrogen column density N_{H} and the optical extinction A_{V} by Güver and Özel (2009) in the galaxy is linear as well.

$$N_{\mathrm{H}}[\mathrm{cm}^{-2}] = (2.21 \pm 0.09) \times 10^{21} \mathrm{A_V[mag]} \tag{19}$$

Therefore not only hydrogen column density N_{H} of the ISM and $E(B-V)$ are proportional, but N_{H} is also proportional to the amount of absorption.

4 XMM-Newton Telescope

In this work I analyzed spectra of BSGs measured by the XMM-Newton telescope of the ESA, which is an x-ray telescope. X-rays can only be observed in space, because the atmosphere blocks out all x-rays. Therefore the XMM-Newton telescope is a space telescope.

The XMM, which stands for x-ray Multi-Mirror Mission, consists of 3 telescopes and an optical monitor (OM). The three telescopes consist of multiple mirrors which are layered. To detect x-rays the mirrors need to be nearly parallel to the path of the x-rays, because of their grating angle. The telescopes use a combination of first parabolic and then hyperbolic surfaces for the mirrors. For detection the XMM-Newton telescopes use 5 different cameras with CCD chips.

Figures 5 and 6 illustarte the construction of the telescopes. There are two systems for detecting the x-ray spectra. For low resolution data the telescope has 3 EPIC Cameras. The MOS1 and MOS2 cameras consist of seven CCD chips each, while the PN camera has twelve CCD chips, which results in a higher count rate in the PN spectrum. The cameras have a range between 0.2 to 10keV (Turner et al., 2001). For high resolution data the Reflection Grating Spectrometers (RGSs) are used. It is a combination of an array of reflection gratings behind two of the telescopes and an RGS camera with CCD Chips in the focus. The two RGS Systems are identical (Brinkman et al., 1998).

The images are processed on-board and generated in x-ray event files. To extract the spectrum out of these event files, one can use the science analysis software (SAS)[3].

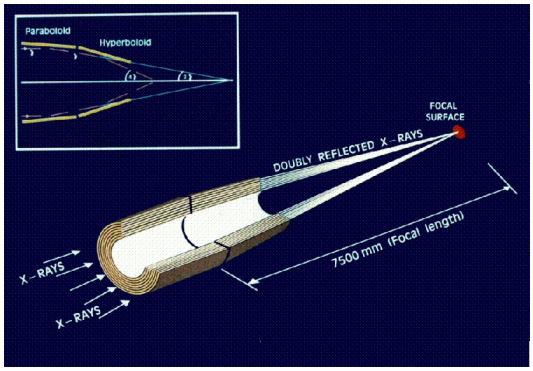

Figure 5: Light path in the XMM-Newton telescope with only an EPIC camera in its primary focus.

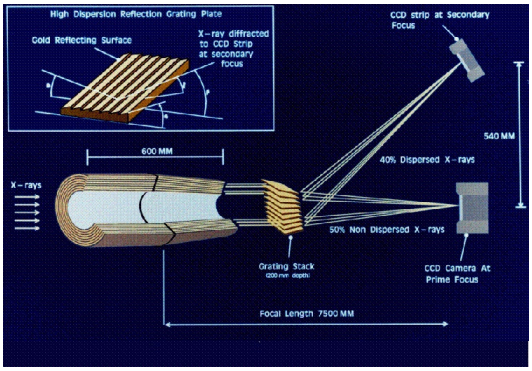

Figure 6: Light path in the two telescopes in which a RGA is mounted into the optical path.

The Figures 5 and 6 and their captions are adapted from the XMM-Newton Webside[4].

[3] `https://www.cosmos.esa.int/web/xmm-newton/sas`
[4] `https://www.cosmos.esa.int/web/xmm-newton/technical-details-mirrors`, 04.07.2021

5 Selection of the sample of B-type stars and their observations

5.1 B-type supergiants

To find suitable stars to analyze for my thesis I used the option 'query by criteria' of the astronomical database SIMBAD[5]. Important was to have stars on both sides of the bi-stability jump. Therefore I selected stars with the criteria: a spectral type of B0, B1 or B2, a luminosity class $splum < II$ and V magnitude $vmag < 8$.

Five of these stars were detected by the XMM-Newton telescope and the target was within less than 5 arcsec from the observation coordinates. This can easily be checked with the XMM-Newton Science archive[6], where I used the catalogs 4XMM-DR10 Filtered Catalog and 4XMM-DR10s Filtered Stack Catalog.

The star HD 14052 was detected by the Chandra x-ray telescope and within 1 arcsec from the observation coordinates, which I found through the 'Quick search' option of the Chandra Source Catalog 2.0[7]. However the count rate of the star was too low to analyze with xspec, so for this star and the stars HD 91969, κ Ori and HD 91943 I just used the parameters from literature. The star HD 152234 I first selected as well, because its spectral type in SIMBAD is displayed as B0.5Ia, but the spectral type in newer papers is specified as O9.7I (Le Bouquin et al., 2017). I decided to include it as well, but also only used parameters retrieved from literature. The log of observations is shown in table 2 and the stellar parameters of all B-type supergiants used in this work are displayed in table 3.

Table 2: Log of observations of BSGs observed by XMM-Newton telescope and analyzed in this work

name (1)	HD number (2)	date of observation (3)	useful exporure time [s] (4)
ϵ Ori	HD 37128	2002-03-06	12260
J Pup	HD 64760	2007-03-16	65300
γ Ara	HD 157246	2004-02-22	22310
θ Ara	HD 165024	2005-10-12	55570
ζ Per	HD 24398	2004-02-13	37320

the dates of the observations (column 3) are from the catalog summery of the PPS data; the useful exposure times (column 4) are given by the xspec program, which I used to analyze the x-ray spectra and every exposure time is for the EPN instrument of the XMM-Newton telescope, except for ϵ Ori, which is the exposure time of the RGS2

[5] `http://simbad.u-strasbg.fr/simbad/`
[6] `http://nxsa.esac.esa.int/nxsa-web/#search`
[7] `https://cxc.cfa.harvard.edu/csc/`

Table 3: Stellar parameters of the sample of early B-type supergiant stars[1] observed by Chandra and XMM-Newton telescopes and analyzed in this work

#	name	HD number	spectral type	Vmag [m]	distance [pc]	$T_{\rm eff}$ [kK]	$log(\frac{L}{L_\odot})$	v_∞ [km/s]	$log(\dot{M})$
(1)	(2)	(3)	(4)	(5)	(6)	(7)	(8)	(9)	(10)
1	HD 152234	HD 152234	O9.7I	5.45	794 ± 397	28.4	5.49		
2	ϵ Ori	HD 37128	B0Ia	1.69	606 ± 166	28.1	5.60	1445	-5.91
3	HD 91969	HD 91969	B0Ib	6.43	2769 ± 366	29.7	5.66	1690	-5.84
4	κ Ori	HD 38771	B0.5Ia	2.06	198 ± 7	24.7	5.58	1445	-5.60
5	J Pup	HD 64760	B0.5Ib	4.24	508 ± 26	25.4	5.58	1390	-6.31
6	HD 91943	HD 91943	B0.7Ib	6.70	3830 ± 496	24.4	5.51		
7	HD 14052	HD 14052	B1Ib	7.787	2129 ± 244	21.7	5.38	1010	-5.76
8	γ Ara	HD 157246	B1Ib	3.34	341 ± 19	21.7	5.38	1010	-5.76
9	θ Ara	HD 165024	B2Ib	3.66	249 ± 10	18.1	5.27	840	-6.01
10	ζ Per	HD 24398	B2Ib	2.85	230 ± 10	18.1	5.27	840	-6.01

All stellar parameters are from SIMBAD, except for the spectral type (column 4) of HD 152234, where the spectral type differs in newer papers from the one displayed in SIMBAD and therefore it is from Le Bouquin et al. (2017). The distances (column 6) are calculated with formula 23, where the parallax π is retrieved from SIMBAD. For the effective temperatures (column 7) of the stars I found two papers, which had a high difference of $T_{\rm eff}$ in B0I stars. However for the other spectral types the effective temperatures match, so I decided to use Searle et al. (2008) for the BSGs and Zorec et al. (2009) for the B-type giants (see table 5). The luminosities (column 8) are from Searle et al. (2008) for all stars as well, except HD 152234, which is from Martins et al. (2005). The mean terminal velocities (column 9) are from Prinja and Massa (1998) and the theoretical mass loss rates (column 10) are calculated with the recipe from Vink et al. (2001).

1 as well as one O-type star

ϵ **Ori** has a high resolution spectrum, which was detected with the Reflection Grating Spectrometer (RGS1 and RGS2) of the XMM-Newton telescope. I could use the Pipeline data (PPS) for this star.
J Pup, γ **Ara and** θ **Ara** have low resolution spectra observed with the MOS1, MOS2 and PN cameras of the XMM-Newton telescope.
ζ **Per** has an EPIC spectrum, but has no PPS data, so I needed to extract the EMOS1, EMOS2 and EPN spectra from the event list using SAS. With that I could extract the spectrum, background spectrum and create the rmf and arf files.
κ **Ori** has an high resolution spectrum and was observed by the Chandra telescope. I used the data for temperatures from table 8 and the luminosity in table 7 from (Cazorla and Nazé, 2017)
HD 91969, HD 91943 and HD 14052 were all observed by Chandra and I just used the luminosity from literature in table 7
The x-ray light curves of all stars are just showing noise and don't give any indication of strong variability. I also checked Fast Fourier Transform spectra provided by PPS but no sign of variability is obvious.

5.2 B-type giants

For comparison purposes I extended the x-ray analysis to B-type giants. Conveniently, the proposal from Waldron (2006) for observation time with the XMM-Newton telescope included five B-type giants. Four of them were detected by the XMM-Newton telescope. I analyzed these stars, to compare them with the supergiants. The star 15CMa I had first included in the sample of B-type supergiants, but discovered later that SIMBAD displayed the wrong spectral type. In SIMBAD the star is identified as spectral type B1Ib, but in recent papers its specified as B1IV (see Burssens et al., 2020). However, I couldn't include the star in the sample B-type giants, because its count rate was too low to analyze the spectrum. The log of observations is shown in table 4 and the stellar parameters for these stars are in table 5.

Table 4: Log of observations of B-type giants observed by XMM-Newton telescope and analyzed in this work

name (1)	HD number (2)	date of observation (3)	useful exporure time PN [s] (4)
Φ^1 Ori	HD 36822	2010-03-14	27330
β CMa	HD 44743	2015-04-21	98000
κ Sco	HD 160578	2008-03-12	54120
γ Ori	HD 35468	2012-09-22	43320

The dates of the observation (column 3) are from the catalog summery of the PPS data. The useful exposure times (column 4) are given by the xspec program and every exposure time is for the EPN instrument of the XMM-Newton telescope.

Table 5: Stellar parameters of the sample of early B-type giant stars observed by XMM-Newton telescopes and analyzed in this work

#	name	HD number	spectral type	Vmag [m]	distance [pc]	$T_{\rm eff}$ [kK]	$log(\frac{L}{L_\odot})$
(1)	(2)	(3)	(4)	(5)	(6)	(7)	(8)
11	Φ^1 Ori	HD 36822	B0III	4.41	333 ± 28	29.07	3.57
12	β CMa	HD 44743	B1II-III	1.97	151 ± 6	24.88	4.38
13	κ Sco	HD 160578	B1.5III	2.386	148 ± 4	24.4	4.07
14	γ Ori	HD 35468	B2III	1.64	77 ± 4	21.74	3.94

All stellar parameters are from SIMBAD, except for the spectral type (column 4) of γ Ori, which is from Burssens et al. (2020). The distances (column 6) are calculated with formula 23, where the parallax π is retrieved from SIMBAD. The effective temperatures (column 7) are from Zorec et al. (2009) and the luminosities (column 8) are from Chandler et al. (2016).

The four B giants I analyzed with xspec had all low resolution spectra detected by the MOS1, MOS2 and PN cameras of the XMM-Newton telescope. But usable data was only obtained to maximal 2 keV, which is different from my sample of supergiant stars. That can be seen in the spectra displayed in section 8.2.

6 X-ray analysis

6.1 Modelling with the xspec program

The xspec program is an x-ray spectral analysis software from Arnaud (1996), which was used in this work to measure x-ray fluxes and plasma temperatures of the sample stars. For analyzing an EPIC spectrum of a star observed with the XMM-Newton telescope not only the file with the spectrum is needed, but also the background spectrum and the arf and rmf files. The software has different models for fitting a spectrum. To analyze the x-ray spectra, I used two models combined, the Tuebingen-Boulder ISM absorption model, which serves as a multiplicative model component and the model of an APEC emission spectrum, which is an additive model. In the following paragraphs are short introductions to these two models used for the x-ray spectra analysis for my sample of stars. All the analyzed spectra in this thesis with their fitting models from the BSGs are in section 8.1 and for the giants in section 8.2

The Tuebingen-Boulder ISM absorption model, known in xspec as *tbabs* model, calculates the absorption of x-rays in the ISM. It has one parameter that can be varied by the user and that is N_{H} the hydrogen column density in units of $[10^{22}\frac{\mathrm{atoms}}{\mathrm{cm}^2}]$. The hydrogen column densities of the ISM of the sample of stars are in table 6. It calculates the x-ray absorption with photoionization cross sections, thereby using typical ISM abundances (for more information see the review for the model from Wilms et al. (2000)).

The APEC emission spectrum model can be used on x-ray emission spectra of optically-thin thermal plasmas, where the emission is dominated by emission through collision. It is based on the AtomDB atomic database[8]. The processes of x-ray emission are described in section 2.2. The *vapec* model is a variant of the *apec* model, where it is possible to vary the metal abundances. Its parameters are plasma temperature kT in [keV], metal abundances, redshift z (for all the sample stars $z = 0$) and $norm$ which is defined as

$$norm_{\mathrm{xspec,T}} = \frac{10^{-14}}{4\pi[d_{\mathrm{A}}(1+z)]^2}\int n_{\mathrm{e}} n_{\mathrm{H}} \mathrm{d}V, \tag{20}$$

with d_{A} as angular distance to the source in [cm], redshift z, n_{e} and n_{H} electron- and H- densities in $[\mathrm{cm}^{-3}]$.

A model APEC spectrum for a typical energy range and plasma temperature is displayed in figure 7. The continuum in the spectrum is due to Bremsstrahlung and the lines are from de-excitation and recombination from electrons.

[8] `http://atomdb.org/`

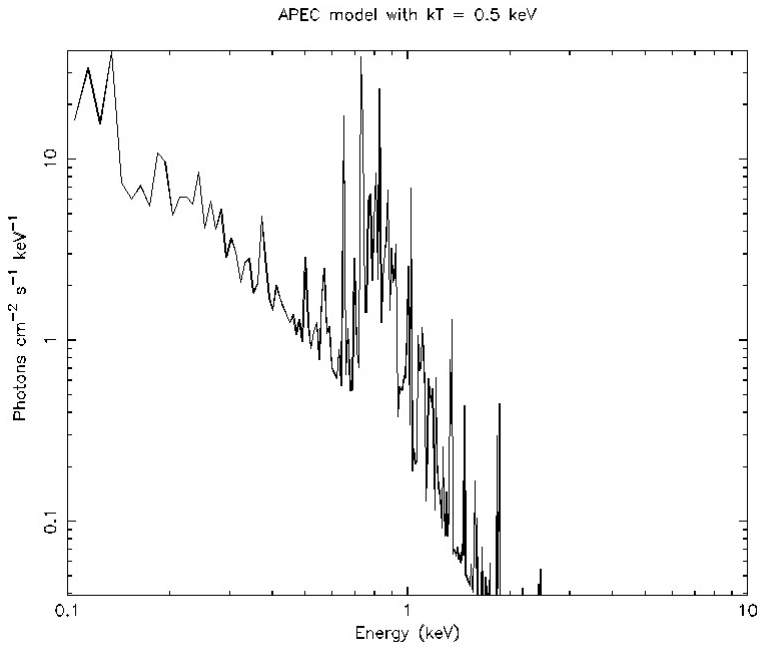

Figure 7: The *apec* model for an energy range of 0.2 - 10.0 keV with a plasma temperature of 0.5 keV, solar metal abundances, redshift $z = 0$ and $norm = 1$.

All the stars in the sample had better fits, when the model had multiple temperatures with corresponding norms. The norms give the amount of plasma with one temperature and the corresponding metal abundances. By varying the metal abundances depending on the biggest deviations from model fit to the spectrum the fit could be improved immensely. By freezing parameters like metal abundances after fitting them, I could decrease the errors of the temperatures and norms. The results on the parameters kT and $norm$ from the models for the stars can be seen in table 9.

Xspec gives the possibility to not only show the absorbed flux, but also calculate the de-reddened flux of a spectrum, by adding the component *cflux* to the model. This model component has three parameters, the minimum and maximum energy, which are fixed so they can not be varied and the logarithmic unabsorbed flux $log_{10}(F_{\mathrm{X}})$ in units of $[\frac{\mathrm{erg}}{\mathrm{s \cdot cm^2}}]$. For my sample stars it is best to use a range of 0.3 - 10 keV to calculate the flux, which is the range of the XMM-Newton telescope.For calculating the flux without a spectrum the High Energy Astrophysics Science Archive Research Center (HEASARC)[9] has an online version of this model called WebPIMMS[10]. Using this additional values for the parameters absorbed flux, as well as N_{H}, and an emission model with corresponding plasma temperature is needed. I used this for the stars κ Ori and HD 14052.

[9] `https://heasarc.gsfc.nasa.gov/`
[10] `https://heasarc.gsfc.nasa.gov/cgi-bin/Tools/w3pimms/w3pimms.pl`

6.2 Results on hydrogen column density

The hydrogen column density N_{H} is an important parameter in fitting an x-ray spectrum, because the spectrum of the star has to be corrected for absorption in the ISM (for further information see 3). Table 6 shows the the reddening E(B-V) (column 3) and the hydrogen column density $N_{H,ISM}$ (column 4) for the sample of stars I analyzed with xspec, both taken from literature, where the reddening due to the ISM is studied. Like described in section 3 and shown in equations 18 and 19 these two parameters should be proportional by an absorption of x-rays in the ISM. However, table 6 clearly shows, that is not the case. For example the stars J Pup and γ Ara have the same value for $E(B-V)$ but a huge difference in $N_{\mathrm{H,ISM}}$. When comparing the two PN spectra of the stars, figure 8 shows that γ Ara has a higher absorption than J Pup. That can be seen in the soft part of the spectrum that gets "eaten" more with higher absorption.

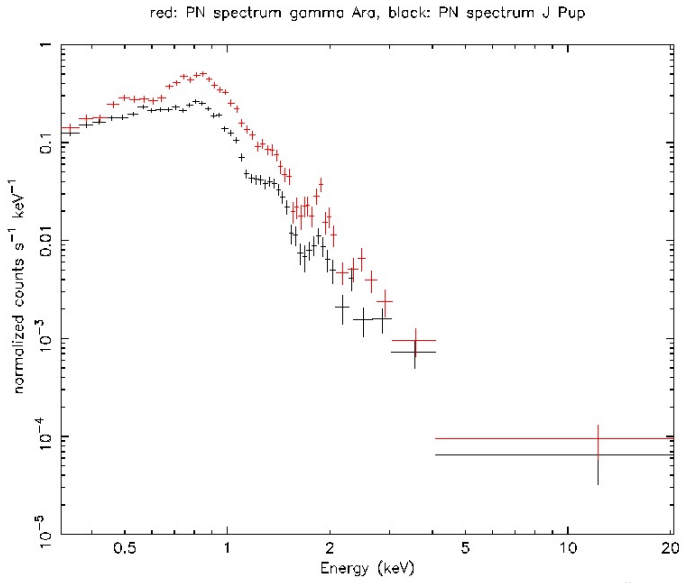

Figure 8: Comparison of the PN spectra of J Pup (black crosses) and γ Ara (red crosses) on a logarithmic y-scale.

Therefore it is a possibility these discrepancies from the typical observation of ISM absorption (see Güver and Özel, 2009) come from absorption of x-rays within the stellar wind, which adds to the absorption from the ISM. When contemplating the continuity equation ρv = const., an increase in density over the bi-stability jump can be assumed, which is due to the drop in terminal velocity v_{∞}. This increase in density could lead to an increase in absorption within the stellar wind. To test the hypothesis of additional x-ray absorption in the stellar wind, I tried adding another absorption model component describing the absorption in the wind to the *tbabs* model with the fixed value of $N_{H,ISM}$ for the ISM absoption. However, with a second *tbabs* model the resulting errors for

the calculated $N_{\mathrm{H,stellarwind}}$ were too high. When exchanging it for an absorption edge model, which calculates the absorption edge with the parameters of a threshold energy E_{c} and an absorption depth D, the program couldn't find an edge in the spectrum. It is likely, that the spectral resolution of the EPIC camera is not sufficiently high for testing the *edge* model.

Therefore, I used my model *tbabs*(vapec+vapec+vapec)*, but letting xspec calculate the values for the hydrogen column densities. The resulting values are in table 6 column 5. Figure 9 compares the values for hydrogen column density of the ISM retrieved from literature $N_{\mathrm{H,ISM}}$ and those calculated with xspec $N_{\mathrm{H,xspec}}$. It shows clearly the excess absorption for later spectral types. That strengthens the theory of absorption of x-rays in the stellar wind, due to an increase in density with later spectral types. It seems therefore, that x-rays are emitted far inside the wind and are absorbed in the wind when propagating toward the observer. When calculating $N_{\mathrm{H,xspec}}$ it is important to know, that by varying metal abundances in the model for the emission of x-rays in the wind, the value of $N_{\mathrm{H,xspec}}$ is changing too. By having so many unknown parameters when fitting the model, it is difficult to find an exact value for N_{H}.

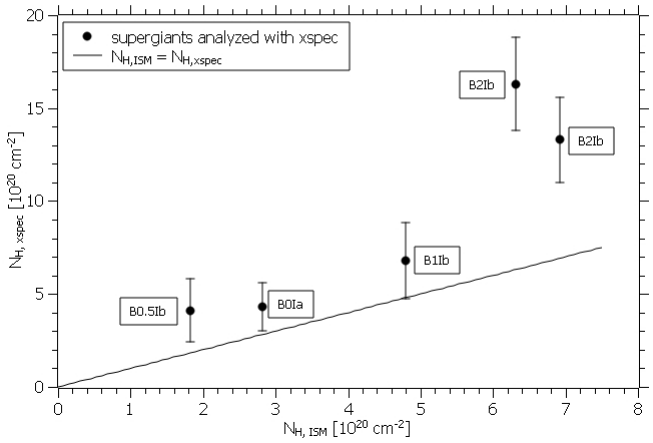

Figure 9: Comparison of the hydrogen column densities $N_{\mathrm{H,ISM}}$ from literature and $N_{\mathrm{H,xspec}}$ for the sample of B-type supergiants analyzed with xspec. The black line marks $N_{\mathrm{H,ISM}} = N_{\mathrm{H,xspec}}$.

As can be seen in figure 10 B-type giants show similar differences between $N_{\mathrm{H,ISM}}$ and $N_{\mathrm{H,xspec}}$ as the BSGs. Deviating from the BSGs though is that the star Φ^1 Ori, which has the earliest spectral type, shows the highest absorption, while later spectral types seem to have less absorption. The fact that $N_{\mathrm{H,xspec}} > N_{\mathrm{H,ISM}}$ fits the theory of x-ray absorption in the stellar winds. However, the highest excess absorption in earlier sprectral types is different to the BSGs and therefore the absorption can't be due to

higher densities in later spectral types. In contrast to BSGs though values for v_∞ for B-type giants are difficult to find and a jump in velocity isn't verified yet (see Waldron, 2006), therefore the density in later spectral types might not be higher.

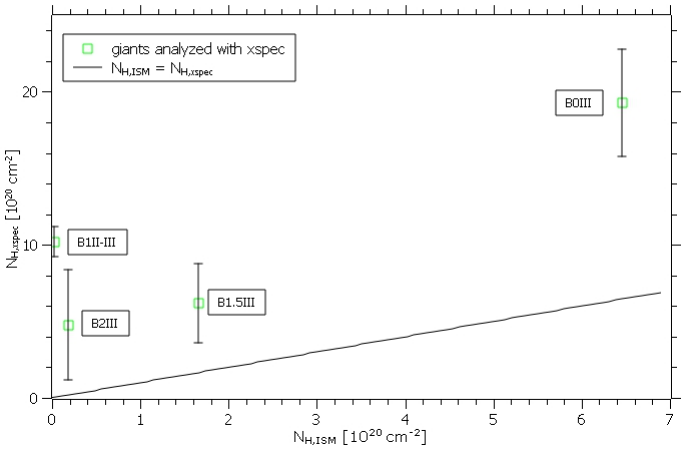

Figure 10: Comparison of the hydrogen column densities $N_{\mathrm{H,ISM}}$ from literature and $N_{\mathrm{H,xspec}}$ for the sample of B-type giants analyzed with xspec. The black line marks $N_{\mathrm{H,ISM}} = N_{\mathrm{H,xspec}}$.

Table 6: Comparison of the hydrogen column densities from literature to the calculated hydrogen column densities with xspec for the sample of stars used for spectral analysis

# (1)	name (2)	$E(B-V)$ (3)	$N_{\mathrm{H,ISM}}$ $[10^{20}\mathrm{cm}^{-2}]$ (4)	$N_{\mathrm{H,xspec}}$ $[10^{20}\mathrm{cm}^{-2}]$ (5)
B-type supergiants analyzed with xspec				
2	ϵ Ori	0.1	2.82	4.3 ± 1.3
5	J Pup	0.05	1.82	4.1 ± 1.7
8	γ Ara	0.05	4.79	6.8 ± 2.03
9	θ Ara	0.06	6.92	13.3 ± 2.3
10	ζ Per	0.27	6.31	16.3 ± 2.5
B-type giants analyzed with xspec				
11	Φ^1 Ori	0.07	6.46	19.3 ± 3.5
12	β CMa	0	0.02	10.2 ± 1.0
13	κ Sco	0	1.66	6.2 ± 2.6
14	γ Ori	0.02	0.18	4.8 ± 3.6

$E(B-V)$ (column 3) and $N_{\mathrm{H,ISM}}$ (column 4) are from Jenkins (2009), except of γ Ori, which is from Berghoefer et al. (1996). $N_{\mathrm{H,xspec}}$ (column 5) is derived from the x-ray spectra of the stars with the model *tbabs*(vapec+vapec+vapec)* from xspec, hereby the model component *tbabs* calculates the hydrogen column density for ISM absorption.

6.3 Results on x-ray luminosities

The X-ray flux corrected for the interstellar reddening could be used to compute X-ray luminosities according

$$L_{\mathrm{X}}\left[\frac{\mathrm{erg}}{\mathrm{s}}\right] = F_{\mathrm{X}}\left[\frac{\mathrm{erg}}{\mathrm{s\,cm^2}}\right] 4\pi d[\mathrm{cm}]^2 \tag{21}$$

$$= 1.2 \cdot 10^{44} d[\mathrm{kpc}]^2 \mathrm{F}_{\mathrm{X}}\left[\frac{\mathrm{erg}}{\mathrm{s\,cm^2}}\right], \tag{22}$$

where d is the distance to the star. The distance of a star is related to their parallax. When a star is close enough to the observer to detect their parallax π, which is the case for all the sample stars, because they are located in our galaxy, it is possible to calculate the distance with

$$d[\mathrm{kpc}] = \frac{1}{\pi[\mathrm{mas}]}. \tag{23}$$

The resulting x-ray luminosities of my sample stars are given in table 7.

Figure 11 shows the x-ray luminosity of the supergiants. It can clearly be seen, that the x-ray luminosities of the BSGs decrease linear with decreasing T_{eff}. This corresponds with the drop in x-ray flux for BSGs with lower T_{eff} Waldron (2006) mentions, though it is a linear decrease instead of a clear drop.

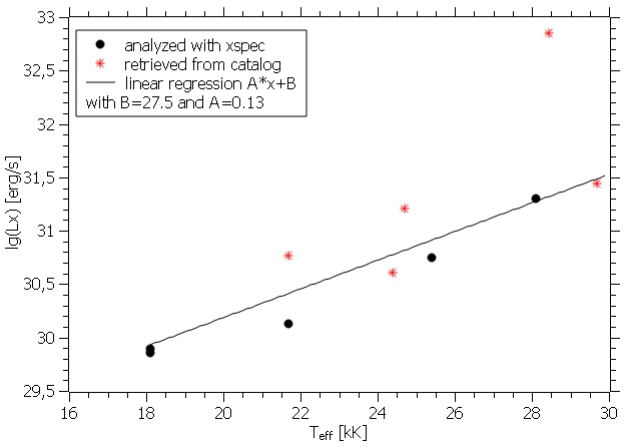

Figure 11: X-ray luminosities (see table 7) plotted against effective temperature (see table 3) for the sample of stars analyzed in this work. The supergiants analyzed with xspec are displayed as black dots and the supergiants retrieved from catalogs as red stars. The black line shows the best fit. The star with the highest x-ray luminosity and $T_{\mathrm{eff}} = 28.4$ is the only O-type star in my sample.

By using equation 15 I can approximate the expected order of magnitude, for an assumed $\kappa(E) = 80\,[\frac{\mathrm{cm}^2}{g}]$ and a $f_\mathrm{X} = 1$, which corresponds with the exospheric approximation in the equation.

$$L_\mathrm{X} \sim 2 \cdot 10^{-23} \frac{\frac{10^{-6}\,\frac{\mathrm{M}_\odot}{\mathrm{yr}}}{1.4 \cdot 10^3\,\frac{\mathrm{km}}{\mathrm{s}}}}{1.3 \cdot 1.14 \cdot (10^{-24}\,\mathrm{g})^2 \cdot 80 \frac{\mathrm{cm}^2}{\mathrm{g}}} \frac{1 + \frac{\pi}{4}}{4} \sim 10^{34} \left[\frac{\mathrm{erg}}{\mathrm{s}}\right] \tag{24}$$

As seen in table 7 this is multiple orders of magnitude too high. This is probably due to the yet unknown factor of the optically depth $\tau_\mathrm{w}(E)$, approximated with a spherical separation, where the mass-absorption coefficient $\kappa(E)$ is different for every star and the high approximation of $v(r) = v_\infty$ in this equation. The deviation from the Lx derived from observations (table 7) could also imply filling factors of hot gas of orders 10^{-2} - 10^{-4}, which appears to be a reasonable number.

Table 7: Unabsorbed fluxes and x-ray luminosities for the sample of stars analyzed in this work

# (1)	name (2)	$log_{10}(F_\mathrm{X})$ $[\frac{\mathrm{erg}}{\mathrm{s\,cm^2}}]$ (3)	x-ray luminosity in $log_{10}(L_\mathrm{X})$ $[\frac{\mathrm{erg}}{\mathrm{s}}]$ (4)
supergiants included in this thesis			
1	HD 152234		32.85
2	ϵ Ori	-12.34 ± 0.48	31.30
3	HD 91969		31.44
4	κ Ori	-11.46	31.21
5	J Pup	-12.74 ± 0.021	30.75
6	HD 91943		30.61
7	HD 14052	-14.08	30.77
8	γ Ara	-12.68 ± 0.11	30.13
9	θ Ara	-13.01 ± 0.04	29.86
10	ζ Per	-12.92 ± 0.08	29.88
B-type giants included in this thesis			
11	Φ^1 Ori	-12.36 ± 0.13	30.77
12	β CMa	-12.038 ± 0.006	30.40
13	κ Sco	-12.85 ± 0.05	29.57
14	γ Ori	-12.89 ± 0.08	28.97

The unabsorbed flux (column 3) has an absorbed flux in the range 0.3 - 10 keV and all are calculated with xspec, except for κ Ori and HD 14052, which are calculated with WebPIMMS. This online program calculates the unabsorbed flux with the absorbed flux, which was for κ Ori from Cazorla and Nazé (2017) and for HD 14052 from Currie et al. (2009) and the hydrogen column density N_H, which was for κ Ori from Jenkins (2009) and for HD 14052 from Evans et al. (2010). The x-ray luminosities (column 4) are calculated with formula 22, except for HD 91969 and HD 91943, which are from Preibisch et al. (2017) and HD 152234, which is from Townsley et al. (2019).

In figure 12 the giants analyzed with xspec are added to the diagram. They show a steeper drop in L_X around the effective temperature $T_{\text{eff}} = 24.5$, than the supergiants. While the values of the x-ray luminosity for spectral type B0 and B1 are nearly similar, later spectral types in giants have much lower values for x-ray luminosities. The lack of information about wind properties of B-type giants makes theoretical predictions of their x-ray properties difficult.

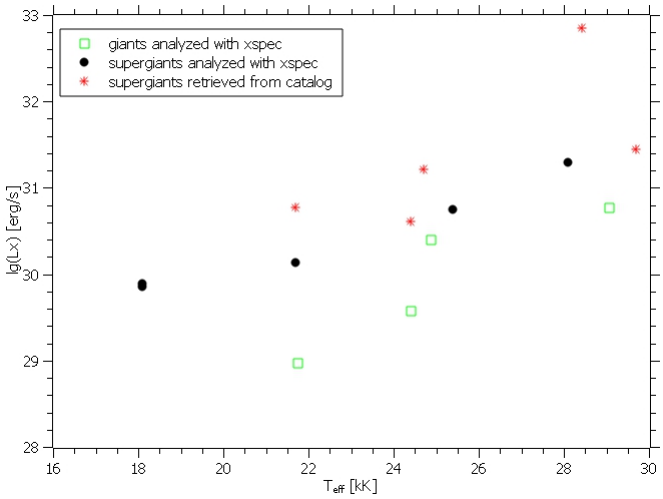

Figure 12: X-ray luminosity of the sample of stars analyzed in this work plotted against their effective temperature T_{eff}. The supergiants analyzed with xspec are displayed as black dots, supergiants retrieved from catalogs as red stars and giants analyzed with xspec as green squares.

6.4 Results on x-ray temperature

The plasma temperatures and corresponding norms of the stellar wind of the sample of supergiants and giants (see table 9) are calculated with the model *vapec* of the xspec program. The best fits were all with three temperatures, except for the star κ Sco, where a model with two temperatures fitted better. Important hereby is that by adding a temperature it is necessary to add the corresponding norm as well. Therefore I added up the *vapec* models depending on the best number of temperatures. Adding more *vapec* model components than three would result in too many unknown parameters for the program to calculate the fit. The average temperatures from these values were calculated with equation 25 and are given in table 8.

$$< kT >= \frac{kT_1\, norm_{T_1} + kT_2\, norm_{T2} + kT_3\, norm_{T_3}}{norm_{T_1} + norm_{T_2} + norm_{T_3}} \tag{25}$$

Hereby it is important to notice that xspec gives a $norm_{\text{xspec,T}}$ dependent on the distance of the star (see equation 20). In order to be able to compare the x-ray temperatures of

the stars, it is necessary to get a $norm_T$ that is not dependent on distance. Therefore

$$norm_T = d^2 norm_{\mathrm{xspec,T}} \tag{26}$$

with d as distance in [cm].

Assuming that x-ray emission is due to shock wave heating of the plasma according to the models from Feldmeier et al. (1995), the plasma temperature follows the equation 3. In that case the shock temperature T_S is proportional to the terminal velocity v_∞. Looking at the behaviour of v_∞ over the jump, T_S should drop in stars with effective temperatures lower than 21000 K and therefore with spectral type B1I and later. However, in figure 13 can be seen that the theoretical shock temperatures are much higher than the results of the plasma temperatures measured using the observed spectra. The theoretical temperatures are only approaching the empirically derived plasma temperatures in the stars with spectral type B2I, hence on the "cool" side of the bi-stability jump. Furthermore the average temperatures of the BSGs don't vary much with later spectral types. Therefore in contrast to the x-ray luminosity, the x-ray temperature doesn't seem to correspond to the change in the wind character. The only star with an unusually high average temperature is γ Ara, which is not to be expected in a B1I star. Even in this star, the empirically measured temperature of X-ray emitting plasma is significantly lower than predicted by the Rankine–Hugoniot shock condition (equation 3).

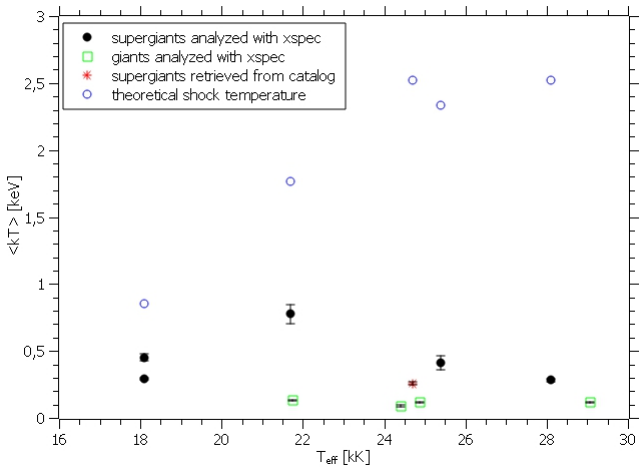

Figure 13: Average temperatures of the x-ray emitting plasma for the sample of stars analyzed in this work (see table 8) plotted against T_eff. The supergiants analyzed with xspec are displayed as black dots, supergiants retrieved from catalogs as red stars and giants analyzed with xspec as green squares. The theoretical shock temperatures are shown as blue circles.

With figure 14 the average temperatures of the BSGs can be compared to the ones of the B-type giants more easily. It shows clearly, that the B-type giants have continually lower temperatures than the supergiants and their average temperatures are nearly constant. However we don't have (like mentioned in subsection 6.3) a varifikation of a jump in v_∞ or solid values for the velocity. Therefore it is difficult to predict theoretical T_S for B-type giants with the Rankine–Hugoniot shock condition (equation 3).

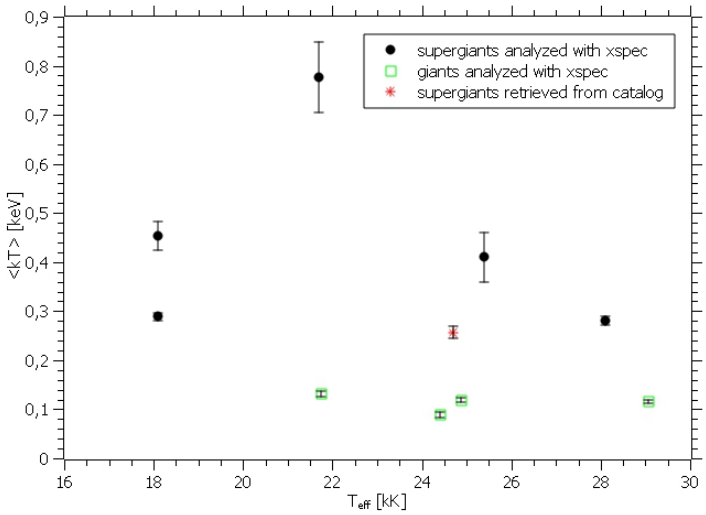

Figure 14: Zoom of figure 13 with average temperature of the x-ray emitting plasma for the sample of stars analyzed in this work (see table 8).The supergiants analyzed with xspec are displayed as black dots, supergiants retrieved from catalogs as red stars and giants analyzed with xspec as green squares.

The theory of shock wave heating can accordingly not explain the behaviour of the x-ray temperatures correctly. Possibly, this is a result of the 1-D nature of the shock models, or of the simplified physics of plasma cooling, which we assume in this work. However, one may also speculate that the shock heating model is not a valid explanation of X-ray emission from the winds of hot stars.

The weighted maximal plasma temperatures of the BSGs don't show high variations with spectral subtype either as can be seen in figure 15. It shows a slow increase with $T_{\rm eff}$, though hereby it has to be considered that especially $< kT_{\rm max}$ of ϵ Ori has high errors and for verification it is necessary to have more observation data for analysis. However, if there actually is an increase with spectral type, this could be related to the behaviour of v_∞. The giants all have lower $< kT_{\rm max} >$ and show in comparison to the supergiants a much clearer increase with $T_{\rm eff}$ and an according decrease with later spectral types.

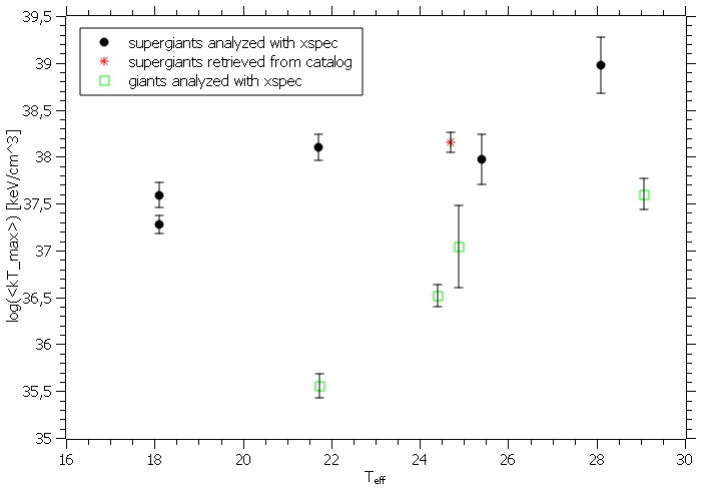

Figure 15: Weighted maximal temperatures of x-ray emitting plasma for the sample stars derived from their x-ray spectra (see table 8) plotted against their effective temperatures. The BSGs analyzed with xspec are displayed as black dots, BSGs retrieved from catalogs as red stars and B-type giants analyzed with xspec as green squares. The displayed errors are the relative errors $\mathrm{d}log_{10}(< kT_{\max} >) = \frac{1}{ln(10)} \frac{\mathrm{d}<\mathrm{kT_{max}}>}{<kT_{\max}>}$.

Table 8: Average plasma temperatures of the x-ray emitting part of the stellar winds for the sample stars

# (1)	name (2)	$< kT >$ [keV] (3)	$< kT_{\max} >$ [10^{37} $\frac{\mathrm{keV}}{\mathrm{cm}^3}$] (4)	kT_{S} [keV] (5)
B-type supergiants				
2	ϵ Ori	0.281 ± 0.009	94.9 ± 65.3	2.52
4	κ Ori	0.26 ± 0.012	14.2 ± 3.4	2.52
5	J Pup	0.41 ± 0.051	9.6 ± 5.8	2.33
8	γ Ara	0.78 ± 0.08	12.6 ± 4.1	1.77
9	θ Ara	0.289 ± 0.008	1.9 ± 0.41	0.85
10	ζ Per	0.45 ± 0.03	3.9 ± 1.2	0.85
B-type giants				
11	Φ^1 Ori	0.116 ± 0.003	4.0 ± 1.5	
12	β CMa	0.119 ± 0.004	1.1 ± 0.2	
13	κ Sco	0.089 ± 0.006	0.33 ± 0.09	
14	γ Ori	0.131 ± 0.006	0.036 ± 0.011	

The average plasma temperature $< kT >$ (column 3) is calculated with formula 25. The weighted maximal plasma temperature $T_{\max}$ (column 4) is calculated with formula $< kT_{\max} >= kT_{\max}\, norm_{T_{\max}}$. The temperatures and norms for both formulas are from table 9, except for κ Ori, which are from Cazorla and Nazé (2017). The theoretical shock temperature (column 5) is calculated with equation 3.

Table 9: Parameters derived from the x-ray spectra of the stars analyzed with xspec

#	name	kT_1 [keV]	$norm_1$ [$10^{-5}\,\mathrm{cm}^{-5}$]	kT_2 [keV]	$norm_2$ [$10^{-5}\,\mathrm{cm}^{-5}$]	kT_3 [keV]	$norm_3$ [$10^{-5}\,\mathrm{cm}^{-5}$]
(1)	(2)	(3)	(4)	(5)	(6)	(7)	(8)
B-type supergiants analyzed with xspec							
2	ϵ Ori	0.12 ± 0.02	68.5 ± 13.01	0.80 ± 0.04	34.1 ± 3.3	0.254 ± 0.006	237.0 ± 10.8
5	J Pup	0.193 ± 0.006	22.4 ± 0.7	0.94 ± 0.094	4.2 ± 1.7	0.61 ± 0.04	13.5 ± 1.5
8	γ Ara	0.186 ± 0.008	9.9 ± 0.4	0.66 ± 0.012	12.0 ± 0.4	2.2 ± 0.3	5.2 ± 0.5
9	θ Ara	0.111 ± 0.005	15.5 ± 2.3	0.42 ± 0.03	5.6 ± 0.5	0.77 ± 0.03	4.2 ± 0.5
10	ζ Per	0.14 ± 0.02	8.54 ± 1.52	0.43 ± 0.06	5.8 ± 2.1	0.70 ± 0.03	11.3 ± 2.0
B-type giants analyzed with xspec							
11	Φ^1 Ori	0.093 ± 0.004	470 ± 80	0.247 ± 0.007	59.4 ± 3.0	0.78 ± 0.05	4.87 ± 0.81
12	β CMa	0.203 ± 0.004	64.3 ± 3.4	0.53 ± 0.02	9.2 ± 0.5	0.08 ± 0.02	240.5 ± 105.2
13	κ Sco	0.082 ± 0.007	113.7 ± 36.0	0.202 ± 0.008	7.8 ± 1.3		
14	γ Ori	0.101 ± 0.0041	38.94 ± 4.41	0.25 ± 0.02	5.8 ± 0.6	0.87 ± 0.06	0.73 ± 0.12

The x-ray temperatures and norms are calculated with xspec with the model *tbabs*(vapec+vapec+vapec)*, with the exception of κ Sco, where I used the model *tbabs*(vapec+vapec)*. The values for N_H from the *tbabs* model component are in table 6 column 5.

7 Discussion and Conclusion

Using the analysis of x-ray spectra from B-type supergiants and giants, I studied their stellar winds, and empirically tested stellar wind theory.

The increasing differences between hydrogen column density N_{H} calculated from fitting observed x-ray spectra and the values of $N_{\mathrm{H,ISM}}$ from literature is interpreted as an absorption of x-rays in the stellar wind. By comparing the x-ray spectra of stars on both sides of the bi-stability jump, there seems to be an increase in absorption from stellar wind in stars on the "cooler" side. This is consistent with the observation of lower terminal velocities v_∞ and is due to higher densities, as well as theoretically predicted higher mass loss rates $\dot{M}$. This possibility of absorption in the stellar winds also indicates that the x-ray emission takes place deep within the stellar wind. However when measuring the hydrogen column density by fitting x-ray spectra, the value of N_{H} is highly dependent on the individual metal abundances. Therefore further studies on this phenomenon will help improve the stellar wind models.

The theory of shock wave heating of parts of the stellar wind developed by Feldmeier et al. (1995) predicts decreasing x-ray temperatures with the decreasing terminal velocity v_∞ at later spectral types. My measurements of plasma temperature from the analysis of observed spectra show nearly constant values and are on the "hot" side of the jump much lower than predicted. That the x-ray temperature doesn't follow the shock wave model from Feldmeier et al. (1995), is possibly due to the lack of a three dimensional model or incorrect model assumption on plasma being heated by the wind shocks. Alternatively, the plasma could be heated by the magnetic processes associated with stellar photosphere, i.e. analogous to the late type active stars. The lack of a drop in T_{X} with the bi-stability jump leads to the conclusion that either the x-ray temperature doesn't depend on v_∞ or other parameters are compensating the drop in terminal velocity.

On the other hand the x-ray luminosity L_{X} shows a steady decrease with lower effective temperatures and accordingly later spectral subtypes. This follows the prediction from Waldron (2006) of a decreasing x-ray flux over the jump. L_{X} depend not only on v_∞ and $\dot{M}$ (which still has differences in their theoretical predicted and empirically derived values) but also on x-ray temperature due to the cooling function $\Lambda(T_{\mathrm{X}}, E)$ and the optical depth of the cool wind τ_{w}, which hasn't been part of a study for the stellar winds of BSGs yet and which receives importance, because of the earlier mentioned possibility of absorption of x-rays in the stellar wind. Therefore it is difficult to calculate an accurate theoretical prediction, which can be compared with the empirical observations of x-ray luminosity. However L_{X} shows a dependence on effective temperature and accordingly spectral subtype.

The x-ray parameters, x-ray temperature and luminosity of giants in comparison to the supergiants are lower, but seem to follow the same behaviour. Though the lack of infor-

mation about v_∞ and models on their bi-stability jump, makes it difficult to compare their empirically derived x-ray parameters with theoretical predicted ones.

In general there is not much data for analysis available and more observations of BSGs with big x-ray telescopes would help to increase the accuracy of distributions of x-ray parameters over the bi-stability jump and the conclusions that can be drawn from them.

Finally, this thesis demonstrates that the spectroscopic analysis of x-ray spectra of BSGs is a valuable tool for studies of these influential stars and their winds.

8 Appendix

8.1 Spectra of supergiants fitted with xspec

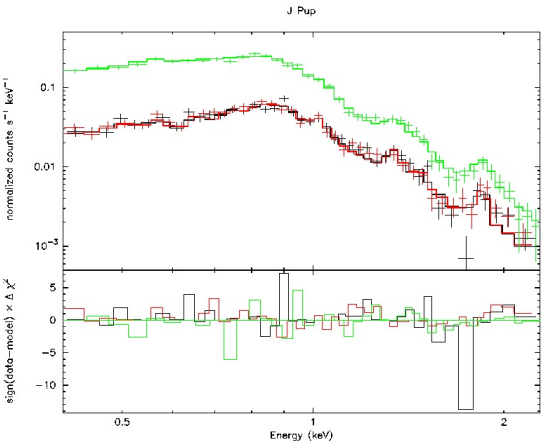

Figure 16: Spectrum of J Pup fitted with xspec with the model *tbabs*(vapec+vapec+vapec)* on a logarithmic y-scale.

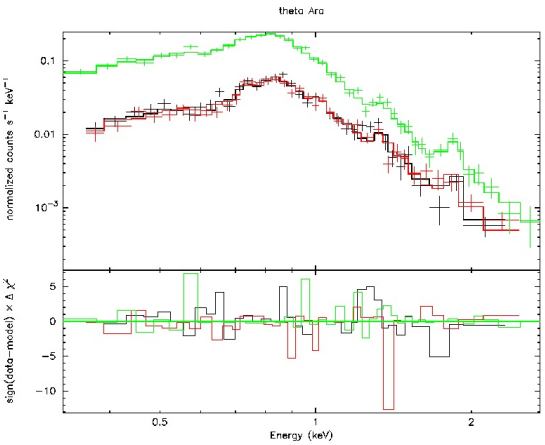

Figure 18: Spectrum of θ Ara fitted with xspec with the model *tbabs*(vapec+vapec+vapec)* on a logarithmic y-scale.

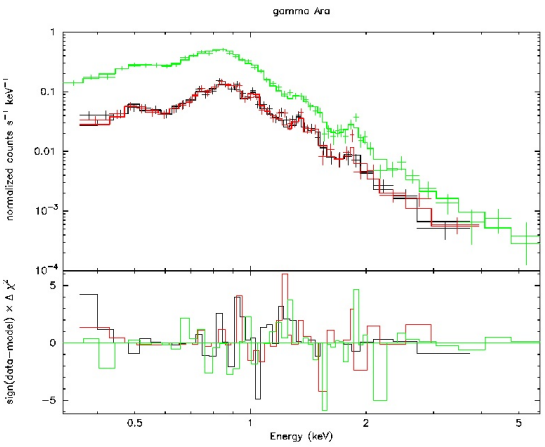

Figure 17: Spectrum of γ Ara fitted with xspec with the model *tbabs*(vapec+vapec+vapec)* on a logarithmic y-scale.

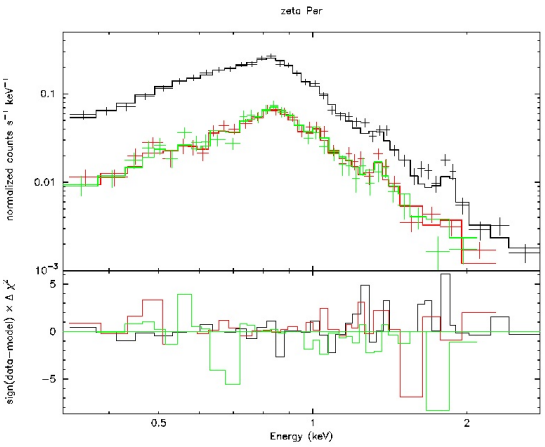

Figure 19: Spectrum of ζ Per fitted with xspec with the model *tbabs*(vapec+vapec+vapec)* on a logarithmic y-scale.

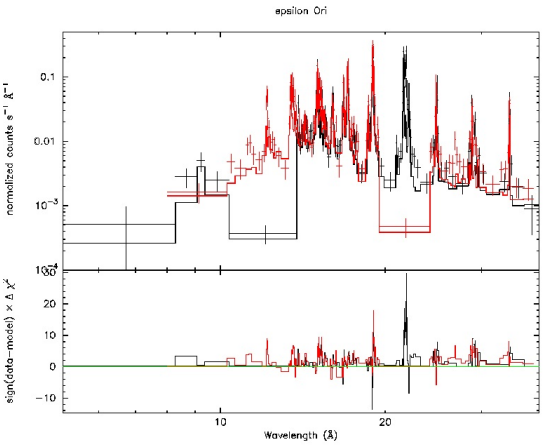

Figure 20: Spectrum of ϵ Ori fitted with xspec with the model *tbabs*(vapec+vapec+vapec)* on a logarithmic y-scale.

8.2 Spectra of giants fitted with xspec

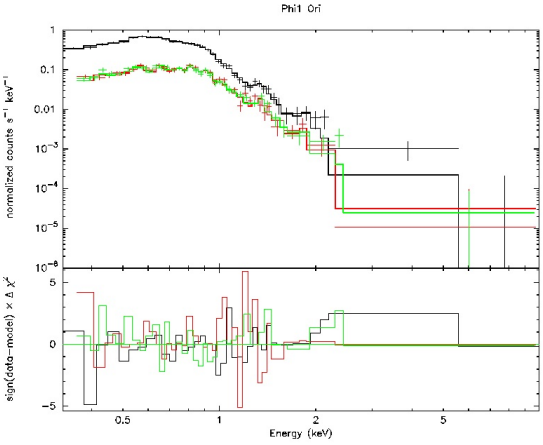

Figure 21: Spectrum of Φ^1 Ori fitted with xspec with the model *tbabs*(vapec+vapec+vapec)* on a logarithmic y-scale.

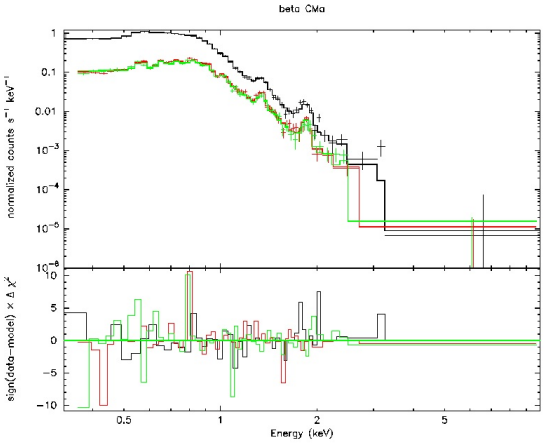

Figure 22: Spectrum of β CMa fitted with xspec with the model *tbabs*(vapec+vapec+vapec)* on a logarithmic y-scale.

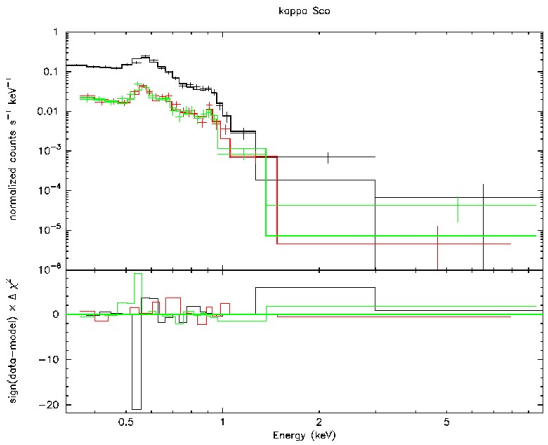

Figure 23: Spectrum of κ Sco fitted with xspec with the model *tbabs*(vapec+vapec)* on a logarithmic y-scale.

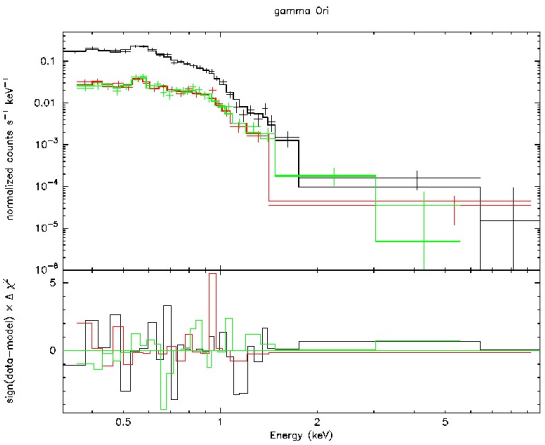

Figure 24: Spectrum of γ Ori fitted with xspec with the model *tbabs*(vapec+vapec+vapec)* on a logarithmic y-scale.

References

K. A. Arnaud. XSPEC: The First Ten Years. In George H. Jacoby and Jeannette Barnes, editors, *Astronomical Data Analysis Software and Systems V*, volume 101 of *Astronomical Society of the Pacific Conference Series*, page 17, January 1996.

T. W. Berghoefer, J. H. M. M. Schmitt, and J. P. Cassinelli. The ROSAT all-sky survey catalogue of optically bright OB-type stars. , 118:481–494, September 1996.

A. Brinkman, H. Aarts, A. den Boggende, T. Bootsma, L. Dubbeldam, J. den Herder, J. Kaastra, P. de Korte, B. van Leeuwen, R. Mewe, F. Paerels, C. de Vries, J. Cottam, T. Decker, S. Kahn, A. Rasmussen, J. Spodek, G. Branduardi-Raymont, P. Guttridge, K. Thomsen, A. Zehnder, and M. Guedel. The Reflection Grating Spectrometer onboard XMM. In *Science with XMM*, page 2, January 1998.

S. Burssens, S. Simón-Díaz, D. M. Bowman, G. Holgado, M. Michielsen, A. de Burgos, N. Castro, R. H. Barbá, and C. Aerts. Variability of OB stars from TESS southern Sectors 1-13 and high-resolution IACOB and OWN spectroscopy. , 639:A81, July 2020. doi: 10.1051/0004-6361/202037700.

Constantin Cazorla and Yaël Nazé. B stars seen at high resolution by XMM-Newton. , 608:A54, December 2017. doi: 10.1051/0004-6361/201731562.

Colin Orion Chandler, Iain McDonald, and Stephen R. Kane. The Catalog of Earth-Like Exoplanet Survey Targets (CELESTA): A Database of Habitable Zones Around Nearby Stars. , 151(3):59, March 2016. doi: 10.3847/0004-6256/151/3/59.

Thayne Currie, Nancy Remage Evans, Brad D. Spitzbart, Jonathan Irwin, Scott J. Wolk, Jesus Hernandez, Scott J. Kenyon, and Jay M. Pasachoff. The X-Ray Environment During the Epoch of Terrestrial Planet Formation: Chandra Observations of h Persei. , 137(2):3210–3221, February 2009. doi: 10.1088/0004-6256/137/2/3210.

S. Ekström, C. Georgy, P. Eggenberger, G. Meynet, N. Mowlavi, A. Wyttenbach, A. Granada, T. Decressin, R. Hirschi, U. Frischknecht, C. Charbonnel, and A. Maeder. Grids of stellar models with rotation. I. Models from 0.8 to 120 M at solar metallicity (Z = 0.014). , 537:A146, January 2012. doi: 10.1051/0004-6361/201117751.

Ian N. Evans, Francis A. Primini, Kenny J. Glotfelty, Craig S. Anderson, Nina R. Bonaventura, Judy C. Chen, John E. Davis, Stephen M. Doe, Janet D. Evans, Giuseppina Fabbiano, Elizabeth C. Galle, II Gibbs, Danny G., John D. Grier, Roger M. Hain, Diane M. Hall, Peter N. Harbo, Xiangqun Helen He, John C. Houck, Margarita Karovska, Vinay L. Kashyap, Jennifer Lauer, Michael L. McCollough, Jonathan C. McDowell, Joseph B. Miller, Arik W. Mitschang, Douglas L. Morgan, Amy E. Mossman, Joy S. Nichols, Michael A. Nowak, David A. Plummer, Brian L. Refsdal, Arnold H. Rots, Aneta Siemiginowska, Beth A. Sundheim, Michael S. Tibbetts, David W. Van Stone, Sherry L. Winkelman, and Panagoula Zografou. The Chandra Source Catalog. , 189(1):37–82, July 2010. doi: 10.1088/0067-0049/189/1/37.

A. Feldmeier, J. Puls, C. Reile, A. W. A. Pauldrach, R. P. Kudritzki, and S. P. Owocki. Shocks and Shells in Hot Star Winds. , 233(1-2):293–299, November 1995. doi: 10.1007/BF00627362.

A. Feldmeier, J. Puls, and A. W. A. Pauldrach. A possible origin for X-rays from O stars. , 322:878–895, June 1997.

Tolga Güver and Feryal Özel. The relation between optical extinction and hydrogen column density in the Galaxy. , 400(4):2050–2053, December 2009. doi: 10.1111/j.1365-2966.2009.15598.x.

Jr. Harnden, F. R., G. Branduardi, M. Elvis, P. Gorenstein, J. Grindlay, J. P. Pye, R. Rosner, K. Topka, and G. S. Vaiana. Discovery of an X-ray star association in VI Cygni (Cyg OB2). , 234:L51–L54, November 1979. doi: 10.1086/183107.

Roberta M. Humphreys, Kris Davidson, David Hahn, John C. Martin, and Kerstin Weis. Luminous and Variable Stars in M31 and M33. V. The Upper HR Diagram. , 844(1):40, July 2017. doi: 10.3847/1538-4357/aa7cef.

R. Ignace and L. M. Oskinova. An explanation of observed trends in the X-ray emission from single Wolf-Rayet stars. , 348:L45–L48, August 1999.

Edward B. Jenkins. A Unified Representation of Gas-Phase Element Depletions in the Interstellar Medium. , 700(2):1299–1348, August 2009. doi: 10.1088/0004-637X/700/2/1299.

Rolf-Peter Kudritzki. *The wind momentum — Luminosity relationship of blue supergiants*, volume 523, page 405. 1999. doi: 10.1007/BFb0106408.

Henny J. G. L. M. Lamers, Theodore P. Snow, and Douglas M. Lindholm. Terminal Velocities and the Bistability of Stellar Winds. , 455:269, December 1995. doi: 10.1086/176575.

J. B. Le Bouquin, H. Sana, E. Gosset, M. De Becker, G. Duvert, O. Absil, F. Anthonioz, J. P. Berger, S. Ertel, R. Grellmann, S. Guieu, P. Kervella, M. Rabus, and M. Willson. Resolved astrometric orbits of ten O-type binaries. , 601:A34, May 2017. doi: 10.1051/0004-6361/201629260.

L. B. Lucy and R. L. White. X-ray emission from the winds of hot stars. , 241:300–305, October 1980. doi: 10.1086/158342.

F. Martins, D. Schaerer, and D. J. Hillier. A new calibration of stellar parameters of Galactic O stars. In F. Casoli, T. Contini, J. M. Hameury, and L. Pagani, editors, *SF2A-2005: Semaine de l'Astrophysique Francaise*, page 351, December 2005.

A. W. A. Pauldrach and J. Puls. Radiation-driven winds of hot luminous stars. VIII. The bistable wind of the luminous blue variable P Cygni (B1 Ia+). , 237:409, October 1990.

Blagovest Petrov, Jorick S. Vink, and Götz Gräfener. On the Hα behaviour of blue supergiants: rise and fall over the bi-stability jump. , 565:A62, May 2014. doi: 10.1051/0004-6361/201322754.

T. Preibisch, S. Flaischlen, B. Gaczkowski, L. Townsley, and P. Broos. Chandra X-ray observation of the young stellar cluster NGC 3293 in the Carina Nebula Complex. , 605:A85, September 2017. doi: 10.1051/0004-6361/201730874.

Raman K. Prinja and Derck L. Massa. A UV Survey of B Supergiants: Time-Averaged Stellar-Wind Properties. 131:218, January 1998.

S. C. Searle, R. K. Prinja, D. Massa, and R. Ryans. Quantitative studies of the optical and UV spectra of Galactic early B supergiants. I. Fundamental parameters. , 481(3): 777–797, April 2008. doi: 10.1051/0004-6361:20077125.

F. D. Seward, W. R. Forman, R. Giacconi, R. E. Griffiths, Jr. Harnden, F. R., C. Jones, and J. P. Pye. X-rays from Eta Carinae and the surrounding nebula. , 234:L55–L58, November 1979. doi: 10.1086/183108.

Randall K. Smith, Nancy S. Brickhouse, Duane A. Liedahl, and John C. Raymond. Collisional Plasma Models with APEC/APED: Emission-Line Diagnostics of Hydrogen-like and Helium-like Ions. , 556(2):L91–L95, August 2001. doi: 10.1086/322992.

Leisa K. Townsley, Patrick S. Broos, Gordon P. Garmire, and Matthew S. Povich. The Massive Star-forming Regions Omnibus X-ray Catalog, Third Installment. , 244(2): 28, October 2019. doi: 10.3847/1538-4365/ab345b.

M. J. L. Turner, A. Abbey, M. Arnaud, M. Balasini, M. Barbera, E. Belsole, P. J. Bennie, J. P. Bernard, G. F. Bignami, M. Boer, U. Briel, I. Butler, C. Cara, C. Chabaud, R. Cole, A. Collura, M. Conte, A. Cros, M. Denby, P. Dhez, G. Di Coco, J. Dowson, P. Ferrando, S. Ghizzardi, F. Gianotti, C. V. Goodall, L. Gretton, R. G. Griffiths, O. Hainaut, J. F. Hochedez, A. D. Holland, E. Jourdain, E. Kendziorra, A. Lagostina, R. Laine, N. La Palombara, M. Lortholary, D. Lumb, P. Marty, S. Molendi, C. Pigot, E. Poindron, K. A. Pounds, J. N. Reeves, C. Reppin, R. Rothenflug, P. Salvetat, J. L. Sauvageot, D. Schmitt, S. Sembay, A. D. T. Short, J. Spragg, J. Stephen, L. Strüder, A. Tiengo, M. Trifoglio, J. Trümper, S. Vercellone, L. Vigroux, G. Villa, M. J. Ward, S. Whitehead, and E. Zonca. The European Photon Imaging Camera on XMM-Newton: The MOS cameras. , 365:L27–L35, January 2001. doi: 10.1051/0004-6361: 20000087.

J. S. Vink, A. de Koter, and H. J. G. L. M. Lamers. On the nature of the bi-stability jump in the winds of early-type supergiants. , 350:181–196, October 1999.

Jorick S. Vink, A. de Koter, and H. J. G. L. M. Lamers. Mass-loss predictions for O and B stars as a function of metallicity. , 369:574–588, April 2001. doi: 10.1051/0004-6361: 20010127.

Jorick S. Vink, I. Brott, G. Gräfener, N. Langer, A. de Koter, and D. J. Lennon. The nature of B supergiants: clues from a steep drop in rotation rates at 22 000 K. The possibility of Bi-stability braking. , 512:L7, March 2010. doi: 10.1051/0004-6361/201014205.

Wayne Waldron. A Study of the Discontinuous Drop in X-ray Emission at Spectral Type B1. XMM-Newton Proposal, October 2006.

J. Wilms, A. Allen, and R. McCray. On the Absorption of X-Rays in the Interstellar Medium. , 542(2):914–924, October 2000. doi: 10.1086/317016.

J. Zorec, L. Cidale, M. L. Arias, Y. Frémat, M. F. Muratore, A. F. Torres, and C. Martayan. Fundamental parameters of B supergiants from the BCD system. I. Calibration of the (λ_1, D) parameters into T_{eff}. , 501(1):297–320, July 2009. doi: 10.1051/0004-6361/200811147.

Zusammenfassung

Blaue Superriesen (BSGs) sind große, heiße und sehr helle Sterne, die sich in ihrer Entwicklung von der Hauptreihe entfernt haben. Eine besonders wichtige Eigenschaft dieser Sterne sind ihre Sternenwinde, welche Massenverlustraten, die aus beobachteten Daten hergeleitet wurden (see Searle et al., 2008), in Größenordnungen von 10^{-8} bis 10^{-6} $M_{\odot}\,\mathrm{yr}^{-1}$ haben. Aufgrund ihrer Stärke spielen die Sternenwinde eine große Rolle bei der Entwicklung der Sterne, sowie der Entwicklung des interstellaren Mediums (ISM), da sie Impuls, Energie und Materie an dieses übertragen. In den Sternenwinden der BSGs wurde beobachtet, dass es einen starken Abfall in der Geschwindigkeit des Windes um den Spektraltypen B1 gibt. Diesen Sprung nennt man bi-stability jump. Er wird oft verwendet um die Eigenschaften der Sternenwinde genauer zu untersuchen, da mit dem bi-stability jump eine Veränderung im Charakter der Winde stattfindet. Da fast alle massiven Sterne emittieren Röntgenstrahlen, deren Quelle das Plasma der Sternenwinde ist. Damit bieten diese ein optimales Werkzeug zur Untersuchung der Winde. Ich habe in dieser Arbeit Röntgenspektren von BSGs um den Spektralbereich des bi-stability jumps analysiert. Die zugrunde liegende Daten wurden aufgenommen von den größten derzeit existierenden Röntgenteleskopen XMM-Newton und Chandra. Das Ziel war die Abhängigkeit der Eigenschaften von Röntgenstrahlen zum Charakter des Windes zu ermitteln und Theorien zur Produktion von Röntgenstrahlen in den Sternenwinden der BSGs zu überprüfen. Dazu habe ich die Plasmatemperaturen der Bereiche des Windes welche Röntgenstrahlen emittieren, sowie die Röntgenhelligkeiten aus den Spektren der Sterne hergeleitet, indem ich diese mithilfe des Programmes xspec analysiert habe. Hierbei wurde deutlich, dass sich die Plasmatemperaturen in den röntgenemittierenden Teilen der Winde nicht mit dem Sprung in der Geschwindigkeit des Windes verändern. Die mittlere Plasmatemperatur ist bei den Stichprobensternen relativ konstant in den Spektralklassen B0 bis B2. Eine Theorie zur Röntgenemission von Feldmeier et al. (1995) besagt, dass eine Instabilität in den Winden zu Schockwellen führt, die das Plasma auf Millionen von Grad erwärmen, was zu Röntgenemission führt. Diese theoretischen Plasmatemperaturen stellten sich jedoch als wesentlich höher heraus, als meine ermittelten mittleren Plasmatemperaturen hergeleitet aus den Röntgenspektren der Stichprobensterne. Weiterhin habe ich die Röntgenhelligkeit untersucht, welche in den Spektralbereichen B0 bis B2 einen deutlichen Anstieg mit ansteigender Effektivtemperatur der Sterne aufzeigt. Zudem liegen Abweichungen zwischen den Werten für die hydrogen column density N_{H} des ISMs in der Literatur und jenen von mir mit xspec ermittelten vor. Aus diesen konnte ich auf eine mögliche Absorption von Röntgenstrahlen innerhalb der Sternenwinde schließen.

Selbstständigkeitserklärung

Hiermit versichere ich, dass ich die vorliegende Bachelorarbeit selbstständig und ohne Hilfe Dritter verfasst habe. Andere als die angegebenen Quellen und Hilfsmittel wurden nicht verwendet. Die den benutzten Quellen wörtlich oder inhaltlich entnommenen Abschnitte sind als solche kenntlich gemacht. Diese Bachelorarbeit hat in gleicher oder ähnlicher Form noch keiner Prüfungsbehörde vorgelegen und wurde auch nicht veröffentlicht.

Potsdam, 07.07.2021 Lea Faber